Available online at www.sciencedirect.com

SciVerse ScienceDirect

www.elsevier.com/locate/matchar

Water droplet behavior on superhydrophobic SiO_2 nanocomposite films during icing/deicing cycles

A. Lazauskas[a,*], A. Guobienė[a,1], I. Prosyčevas[a,1], V. Baltrušaitis[a,1], V. Grigaliūnas[a,1], P. Narmontas[a,1], J. Baltrusaitis[b,2]

[a]Institute of Materials Science, Kaunas University of Technology, Savanorių 271, 3009 Kaunas, Lithuania
[b]PhotoCatalytic Synthesis Group, University of Twente, Meander 229, P.O. Box 217, 7500 AE Enschede, The Netherlands

ARTICLE DATA

Article history:
Received 17 January 2013
Received in revised form
25 April 2013
Accepted 26 April 2013

Keywords:
Superhydrophobic surface
Icing/deicing
Morphology
Contact angle
AFM

ABSTRACT

This work investigates water droplet behavior on superhydrophobic (water contact angle value of 162 ± 1°) SiO_2 nanocomposite films subjected to repetitive icing/deicing treatments, changes in SiO_2 nanocomposite film surface morphology and their non-wetting characteristics. During the experiment, water droplets on SiO_2 nanocomposite film surface are subjected to a series of icing and deicing cycles in a humid (~70% relative humidity) atmosphere and the resulting morphological changes are monitored and characterized using atomic force microscopy (AFM) and contact angle measurements. Our data show that the formation of the frozen or thawed water droplet, with no further shape change, on superhydrophobic SiO_2 nanocomposite film, is obtained faster within each cycle as the number of the icing/deicing cycles increases. After 10 icing and deicing cycles, the superhydrophobic SiO_2 nanocomposite film had a water contact angle value of 146 ± 2° which is effectively non-superhydrophobic. AFM analysis showed that the superhydrophobic SiO_2 nanocomposite film surface area under the water droplet undergoes gradual mechanical damage during the repetitive icing/deicing cycles. We propose a possible mechanism of the morphological changes to the film surface that take place during the consecutive icing/deicing experiments.

1. Introduction

Undesired ice accumulation on surfaces can lead to significant economic losses as well as safety concerns. Condensation occurs when water vapor, in contact with a cold surface, cools and turns into water droplets. If the surface temperature is lower than the freezing point of water, the water droplets formed on the surface will freeze and form ice, which will result in increase of surface weight, heat transfer resistance and pressure loss. Commonly, anti-icing systems rely on active deicing methods, such as application of heat or mechanical techniques. A more attractive approach is the use of passive methods which do not need external energy for deicing while preventing ice accumulation. These methods include surface modification techniques or coating with material capable of disrupting the structure of the ice. A recent review [1] on advanced icephobic coatings has outlined three families of materials best suited to achieve anti-icing functionality of the surface. Among those, superhydrophobic surfaces have already demonstrated non-wetting behavior, fluid friction reduction, anti-stiction and self-cleaning functionality [2] and

* *Corresponding author*. Tel.: +370 671 73375 (mobile); fax: +370 37 314423.
E-mail addresses: Algirdas.LAZAUSKAS@stud.ktu.lt (A. Lazauskas), Asta.GUOBIENE@ktu.lt (A. Guobienė), IGORPROS@mail.ru (I. Prosyčevas), fei@fei.lt (V. Baltrušaitis), Viktoras.GRIGALIUNAS@ktu.lt (V. Grigaliūnas), Pranas.NARMONTAS@ktu.lt (P. Narmontas), j.baltrusaitis@utwente.nl (J. Baltrusaitis).
[1] Tel.: +370 37 31 3432; fax: +370 37 314423.
[2] Tel.: +31 53 489 3968; fax: +31 53 489 2882.

1044-5803/$ – see front matter © 2013 Elsevier Inc. All rights reserved.
http://dx.doi.org/10.1016/j.matchar.2013.04.017

have already attracted increasing attention because of their potential applications in anti-icing [3–5]. However, it was shown [6,7] that the anti-icing performance of superhydrophobic surfaces may be limited and should be studied in detail with focus on structure–property relationship, with emphasis on surface morphology and their mechanical properties as well as on icing/deicing mechanisms.

Superhydrophobic properties of SiO_2 nanoparticle-containing nanocomposite films have been demonstrated previously [8–10], but the durability of the films and their anti-icing performance have not been adequately examined. In this study, water droplet behavior on superhydrophobic SiO_2 nanocomposite films was examined by applying 30 surface icing/deicing cycles to evaluate the changes in film surface morphology and non-wetting characteristics as well as to estimate their anti-icing suitability.

2. Material and Methods

2.1. *Preparation of Superhydrophobic SiO_2 Nanocomposite Films*

Sol–gel synthesis of colloidal SiO_2 nanoparticles was performed via base catalyzed hydrolysis of tetraethyl orthosilicate (TEOS). A detailed description of SiO_2 sol preparation can be found elsewhere [11]. Briefly, the required amounts of water and ammonium hydroxide were added to the required volume of a 70% solution of denatured ethanol. The resulting mixture was added to TEOS while continuously stirring at 25 °C. The final solution was stored for 7 days at room temperature to allow complete hydrolysis.

A commercially available lithium aluminosilicate glass-ceramic (Alkor Technologies) of 1 mm thickness was used in this study. Before use, it was cut into 2.5 cm × 4.5 cm slides. Glass-ceramic surface preparation included cleaning in 0.1 N hydrochloric acid followed by 0.1 N sodium hydroxide solution. Afterwards, the slides were rinsed with distilled water, then with isopropyl alcohol and dried with compressed air.

The nanocomposite SiO_2 films were prepared on lithium aluminosilicate glass-ceramic slides by spin-coating (spin speed ~ 3000 rpm and spinning time 30 s) using 5 ml of the final SiO_2 sol product and 4 ml of polypropylene glycol [MW ~ 2500] mixture followed by heat-treatment at two different temperatures, 250 and 500 °C for 30 and 60 min, respectively. Spin-coating and heat-treatment procedures were repeated three times. Further modification of SiO_2 nanocomposite films was performed by boiling the spin coated samples in 10% solution of hexamethyldisilazane in toluene for 20 min. Afterwards, the samples were rinsed with ethanol followed by distilled water and dried at 80 °C for 20 min, resulting in the final superhydrophobic film. The process diagram for preparation of the superhydrophobic SiO_2 nanocomposite films is shown in Fig. 1.

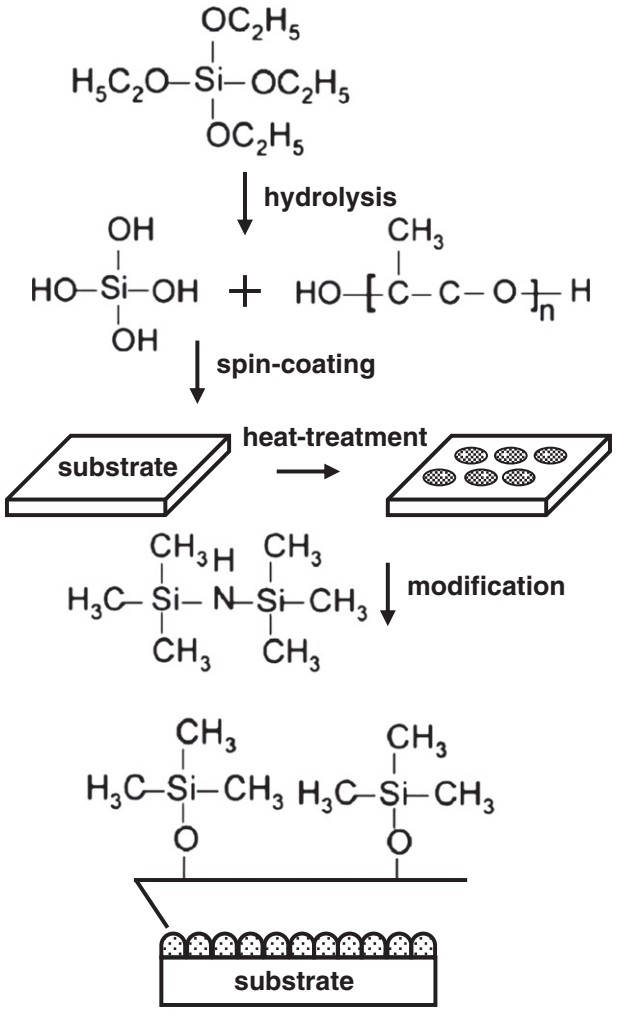

Fig. 1 – Process diagram for the superhydrophobic SiO_2 nanocomposite film preparation.

2.2. *Icing/Deicing Apparatus Experimental Setup*

The experimental setup consisted of a Peltier-based thermo-electric cooler (STONECOLD, PM-30X30-36; 14.6 V; 4.3 A; 36 W) connected to a dc voltage supply controlled by a computer. The bottom side of the lithium aluminosilicate glass–ceramic substrate is attached to the cold side of the thermo-electric cooler using a heat transfer paste (Fixapart, WPS-1GRAM) which ensures rapid heat transfer between the thermo-electric cooler and the substrate. Similarly, a layer of heat transfer paste is applied between the hot side of the thermo-electric cooler and a large aluminum heat sink (82 × 70 × 25 mm^3) ensuring that the stray heat generated on the hot side of the thermo-electric cooler is readily transferred away. A thermocouple (MASTECH, K type) was used to monitor cold side surface temperature of the thermo-electric cooler which was varied from 15 to −15 °C throughout the experiments. A high-speed camera (Manhattan, 500 SX) was used to monitor and record the water droplet shape transition during icing/deicing cycles.

2.3. *Icing/Deicing Experimental Procedure*

Superhydrophobic SiO_2 surface icing/deicing experiments were initiated at the temperature of 15 ± 1 °C and relative humidity of 70 ± 3%. One droplet of deionized water (5 μl) was carefully placed on top of the superhydrophobic SiO_2 nanocomposite film surface. The position of the deposited water droplet on the sample surface was chosen to correspond to the center of the

thermo-electric cooler cold side. Next, surface temperature was changed at a rate of ~0.5 °C/s to −15 °C thus initiating a gradual surface icing process. Complete freezing was considered when no further change in droplet shape could be observed. After the complete freezing of a frozen water droplet, temperature was changed back to 15 °C and thus a gradual SiO_2 surface deicing process took place. Surface temperature and video recordings were made from the moment of SiO_2 surface–water droplet contact until the formation of the thawed water droplet. Afterwards, the water droplet was removed by manually touching the top of the water droplet with a highly water absorbent clean swab head. The SiO_2 nanocomposite surface was then air-dried at room temperature for 24 h. Atomic force microscopy (AFM) measurements were then performed, as well as analysis of captured video. The described experimental procedure was repeated 30 times.

2.4. *Contact Angle Measurements*

Four images of captured video were chosen for contact angle (CA) measurements: at the initial water droplet contact (denoted as CA1); after the initial shape change of the water droplet before turning fully opaque (denoted as CA2); of frozen water droplet with no further deformation in shape (denoted as CA3); and of the thawed water droplet with no further shape change (denoted as CA4). The images of the water droplets were magnified and contact angles were measured using a method based on B-spline snakes (active contours). This method offers the best tradeoff between the use of the general droplet shape to guide the detection of the contour of the drop and the use of an algorithm with local behavior to compute contact angles with high-accuracy [12].

2.5. *AFM Measurements*

AFM experiments were conducted in air at room temperature using a Microtestmachines NT-206 atomic force microscope, while data was analyzed using SurfaceView scanning probe microscopy data processing software. Topographical images were collected using a V-shaped silicon cantilever (spring constant of 3 N/m, tip curvature radius of 10.0 nm and the cone angle of 20°) operating in the contact image mode with 4 μm × 4 μm scan size.

Surface morphology was evaluated using AFM surface topography images. In particular, roughness parameters, root mean square (RMS), roughness (R_q), skewness (R_{sk}) and kurtosis (R_{ku}), height distribution histograms, bearing ratio curves and surface profiles were used. RMS roughness is the average of measured height deviations taken within the evaluation area and measured from the mean linear surface. Skewness parameter indicates surface symmetry within the evaluation area. Negative skewness indicates a predominance of valleys and a positive value indicates a surface having more peaks. Kurtosis is a measure of the randomness of heights, as well as the sharpness of a surface. For a Gaussian-like surface it has a value of 3 [13]. The farther the result is from 3, the less random and more repetitive the surface is. Height distribution histograms show the share of the surface points located at a given height relative to the total number of surface points in percent. Bearing ratio curve is defined as the dependence of the solid material occurrence on the feature height. To obtain more detailed information about the morphology of the surfaces, we defined hybrid parameters of the bearing ratio curve by dividing it into three regions [14]. The upper region of the bearing ratio curve indicates the portion of the surface structures (i.e. peaks) which would be first affected during the contact with another surface and is defined as reduced peak height, R_{pk}. The middle region of the bearing ratio curve indicates the portion of the surface structures responsible for the stiffness characteristics, performance and life of the surface during wear and is defined as core-roughness, R_k. The lower region of bearing ratio curves exhibits surface structures (i.e. valleys) where water molecules adsorbed from the atmosphere could condense or air gaps between the contacting surfaces could emerge affecting the surface adhesive properties, as well as their frictional performance and is defined as reduced valley depth, R_{vk}.

3. Results and Discussion

The mixture of SiO_2 sol and polypropylene glycol can be seen as an inorganic/organic hybrid where phase separation does not occur at room temperature, while it does at higher temperatures. In fact, after the first heat-treatment of the sample at 250 °C for 30 min, phase separation was observed on the surface with the apparent SiO_2 spheres. With the second heat-treatment of the sample at 500 °C, pyrolysis of polypropylene glycol took place with the resulting formation of SiO_2 nanocomposites. CA of the superhydrophobic SiO_2 nanocomposite film was equal to 153 ± 1°, while after modification with a 10% solution of hexamethyldisilazane in toluene it increased to 162 ± 1°. An AFM topographical image of the resulting superhydrophobic SiO_2 nanocomposite film surface is presented in Fig. 2a. It shows that the surface of the superhydrophobic SiO_2 nanocomposite film is rough (R_q: 58.6 nm) composed of randomly distributed micrometer-scale morphological features decorated with nano-sized protrusions. A positive R_{sk} value of 0.19 was calculated for superhydrophobic SiO_2 nanocomposite films indicating a regime where surface peaks dominate the valleys. The SiO_2 nanocomposite film was found to have Gaussian-like surface feature distribution corresponding to R_{ku} value of 2.82, which confirms the random distribution of surface structures. Fig. 2b shows a height distribution histogram and bearing ratio curve of the corresponding SiO_2 nanocomposite film surface (Fig. 2a). A closer look at Fig. 2b shows the presence of nano-sized protrusions on the surface. The superhydrophobic SiO_2 nanocomposite film surface had R_{pk}, R_k and R_{vk} values equal to 66.34, 130.92 and 45.38 nm with the corresponding surface structure height in the range of ~213–279, ~82–213 and ~36–82 nm, respectively.

Fig. 3 (top) shows the temperature of the thermo-electric cooler cold side versus time during the number of icing/deicing cycles. Vertical lines indicate positions at which CA1, CA2, CA3 and CA4 were observed. It is evident that the formation of the frozen or thawed water droplet with no further shape change on superhydrophobic SiO_2 nanocomposite film is obtained faster within each cycle as the number of the icing/deicing cycles increases. Fig. 3 (bottom) shows the change in water contact angle on the superhydrophobic SiO_2 nanocomposite film surface during the 1st, 10th, 20th and 30th icing/deicing cycles.

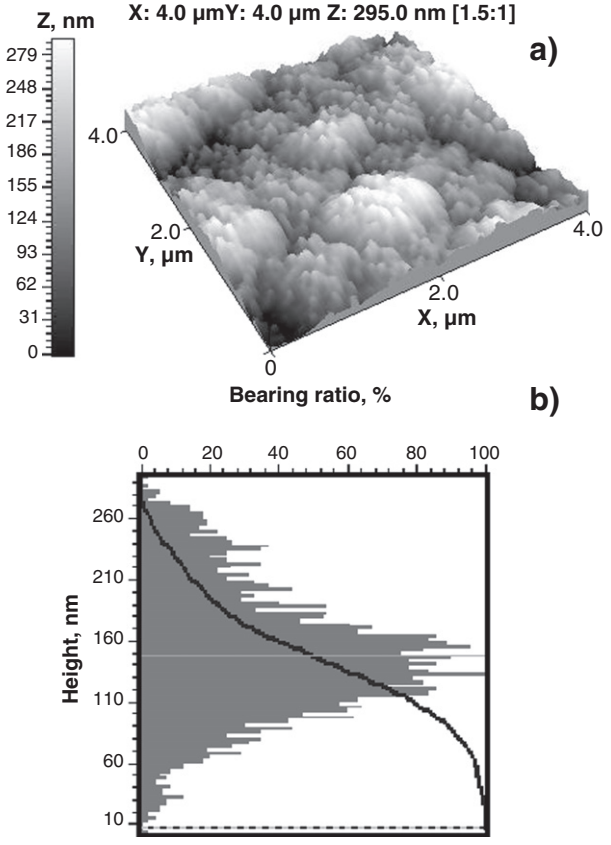

Fig. 2 – (Top) Characteristic AFM topographical image with a normalized z axis in nm (a) as well as (bottom) normalized height distribution histogram and bearing ratio curve (b) of superhydrophobic SiO_2 nanocomposite film. Dashed horizontal line in height distribution histogram indicates the height at which surface structures are connected to each other. The solid horizontal line indicates the mean height.

CA1 value of water droplets placed on superhydrophobic SiO_2 nanocomposite film during the 1st icing/deicing cycle is 162 ± 1°, implying that the water droplet is situated on top of the textured surface with trapped air underneath, evident of the Cassie–Baxter wetting regime [15]. It is clear from Fig. 3 (bottom) that non-wetting properties of superhydrophobic SiO_2 nanocomposite films gradually deteriorate with repeated droplet exposures, which can be seen in the steadily decreasing CA1 values for 10th, 20th and 30th icing/deicing cycles. Importantly, after having been artificially iced and deiced 10 times, the sample demonstrated a CA value of 146 ± 2°, thus no longer behaving in a superhydrophobic manner. The shape change of the water droplet during the gradual icing process was observed in Fig. 3 (bottom, CA1 to CA2), which could be attributed to the thermodynamic instability of air pockets trapped under the water droplet and the corresponding nucleation of water thus minimizing the droplet surface energy [16], implying that wetting transition to a mixed Wenzel and Cassie–Baxter regime [17]. After the wetting transition, no further shape changes of water droplets were observed (CA2 contact angle values in Fig. 3) and several seconds later, water droplets turned fully opaque. It took longer to achieve a stable shape of the water droplet during the initial icing/deicing than during the later steps, showing that the surface had more air pockets trapped under the water droplet, decreasing heat transfer from the cold side of the thermo-electric cooler.

Finally, with further surface icing process (CA2 to CA3), a mushy freezing front [18] was observed, which moved continuously from the bottom to the top of the water droplet with corresponding shape deformation until the whole droplet was frozen and a protrusion formed on the top. Afterwards, no further droplet deformation was observed (CA3 contact angle values in Fig. 3). The phase transition expanded the droplet upwards with no sideways expansion noticeable although the contact angle appeared to have decreased after freezing, which is in a good agreement with previous studies [19,20]. Similarly, it is suggested that during the first tests, the surface had more air pockets trapped under the fully opaque droplet, which decreased propagation of the mushy freezing front and increased the time required to achieve full phase transition. Shape change of water droplet during the gradual surface deicing process (CA3 to CA4) was observed before the steady state of the liquid droplet was achieved. As a result, the CA4 values in Fig. 3 decreased even more compared to those of CA3.

Additional water droplet shape changes observed during the CA3 to CA4 transition could be attributed to the SiO_2 nanocomposite film surface morphological changes arising with ice expansion during the freezing process. Analysis of the water droplet contact angle change is further supported by AFM data (Fig. 4a, b and c) of the superhydrophobic SiO_2 nanocomposite film surface measured after the 10th, 20th and 30th icing/deicing cycles. The RMS roughness (R_q) value of the superhydrophobic SiO_2 nanocomposite film surface increased with the number of icing/deicing cycles performed, suggesting that the R_q parameter alone is insufficient to predict surface wetting behavior. It can be seen that as the surface of the superhydrophobic SiO_2 nanocomposite film is subjected to repetitive icing/deicing treatments, its skewness (R_{sk}) and kurtosis (R_{ku}) decrease systematically, indicating that the nano-sized protrusions responsible for the non-wetting characteristics are damaged and spiky surface morphology is evolving into a bumpy surface morphology [21]. Moreover, after having been artificially iced and deiced 30 times, the negative R_{sk} value of −0.20 was observed, indicating that surface peaks no longer dominate over valleys. This observation is further supported by the AFM topography images and quantified using height distribution histograms, bearing ratio curves and R_{pk} values (Fig. 4). Importantly, the height distribution after the icing/deicing experiments shown in Fig. 4 becomes more uniform than that of the initial superhydrophobic SiO_2 nanocomposite film shown in Fig. 2b.

Based on our experimental results, in Fig. 5 we propose a mechanism of the superhydrophobic SiO_2 nanocomposite film surface morphological changes taking place over a number of the icing/deicing experiments. When a water droplet on the superhydrophobic SiO_2 nanocomposite film begins to solidify and turn to ice, some portions of the nano-sized protrusions indent the forming ice and are mechanically damaged (i.e. cracked or spalled) due to the compressive stress generated during ice expansion. After the formation of the thawed water droplet, the damaged part of the nano-sized protrusions is removed together with the water droplet. Water is then able to get into contact with micrometer-scale surface features observed

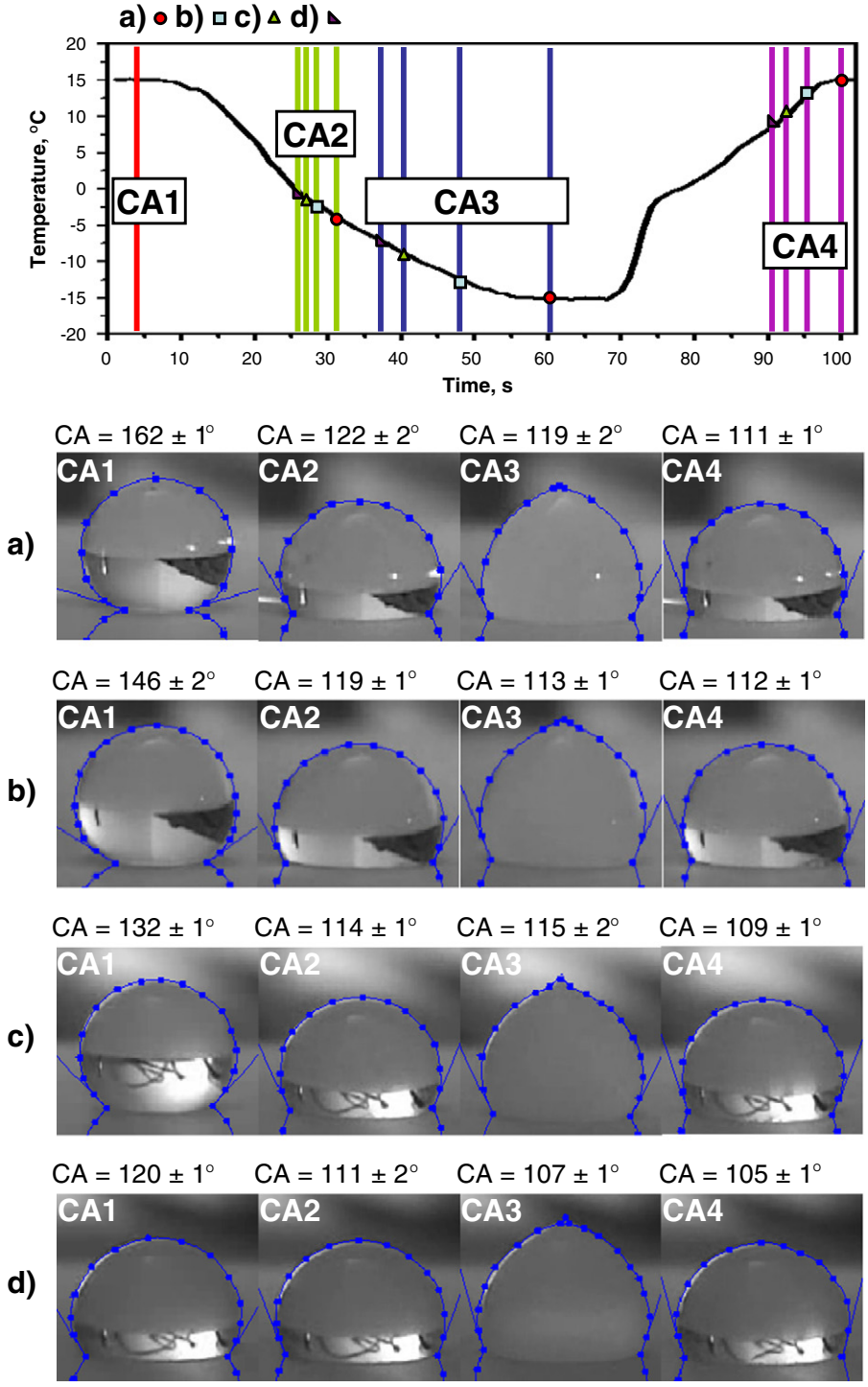

Fig. 3 – (Top) Plot of the temperature of the thermo-electric cooler cold side versus the time during the repeated icing/deicing cycle. Vertical lines indicate positions at which CA1, CA2, CA3 and CA4 were observed during (a) 1st, (b) 10th, (c) 20th and (d) 30th icing/deicing cycles. (Bottom) Variation of water contact angle on the superhydrophobic SiO_2 nanocomposite film surface during the corresponding icing/deicing cycle.

in topographical AFM images when the surface is subjected to a number of icing/deicing treatments. A certain amount of force is generated and thus stress concentrations in the areas of the contact with micrometer-scale structures appear during ice expansion. As a result, micrometer-scale structures undergo deformation which induces stress concentrations in the part of the surface where the micrometer-scale structures are connected to one another, causing the initial crack front formation. Water is then able to nucleate even deeper within the damaged surface which explains the shape change during the formation of the thawed water droplet and the decrease of the corresponding CA values (CA4 values in Fig. 3). As additional surface icing/deicing cycles occur, the crack front propagates. It increases the surface area and performs the change in surface height distribution as

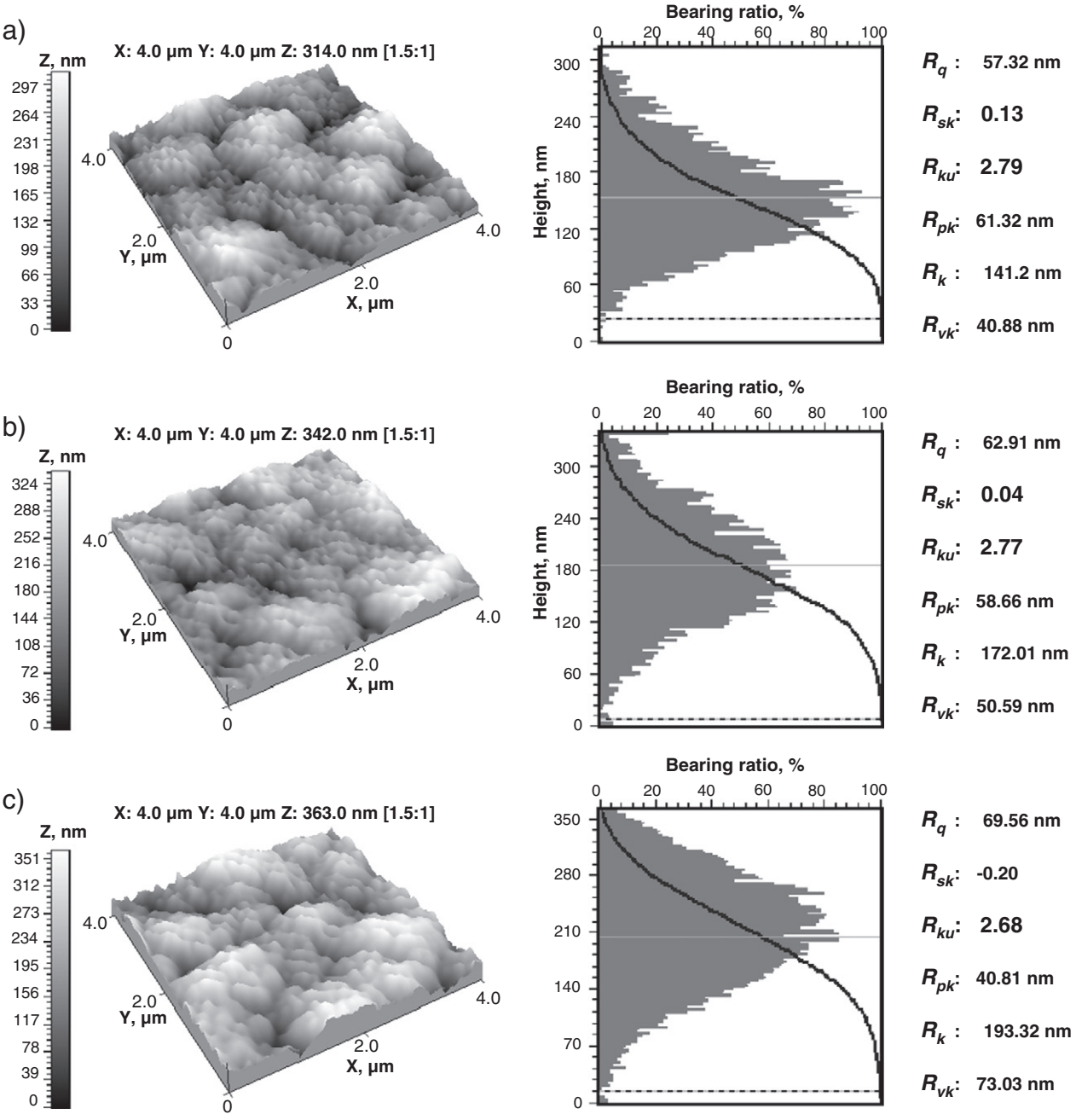

Fig. 4 – Characteristic AFM topographical images with the normalized z axis in nm; normalized height distribution histograms and bearing ratio curves as well as surface morphology parameters of superhydrophobic SiO_2 nanocomposite film after (a) 10th, (b) 20th and (c) 30th icing/deicing cycles. Dashed horizontal line in height distribution histogram indicates the height at which surface structures are connected to each other. The solid horizontal line indicates the mean height.

well as the quantitative behavior of the surface morphological parameters. The model presented in Fig. 5 is consistent with the behavior of both measured CA values and observed surface morphological changes.

Our data indicate that superhydrophobic SiO_2 nanocomposite films alone are not sufficiently durable to be used for anti-icing applications in humid environments. The surface undergoes gradual mechanical damage and looses its non-wetting characteristics during repetitive icing/deicing cycles, thus ice adhesion strength is expected to increase as water repellency constantly deteriorates.

Despite the economic significance of having effective ice-repellent materials, state-of-the-art anti-icing films/surfaces are still far from optimal, as frost and ice can easily build up even under moderate icing conditions (e.g., <5 °C with relative humidity > 50%) [22]. In a recent study by L. Mishchenko et al. it was demonstrated in detail that under low humidity conditions superhydrophobic surfaces can indeed be effective as ice-repellent materials [23]. However, it was also shown in [24] that superhydrophobic surfaces, typically having nano- or micro-scale roughness, may induce ice nucleation at an even faster rate than smooth surfaces of the equivalent materials

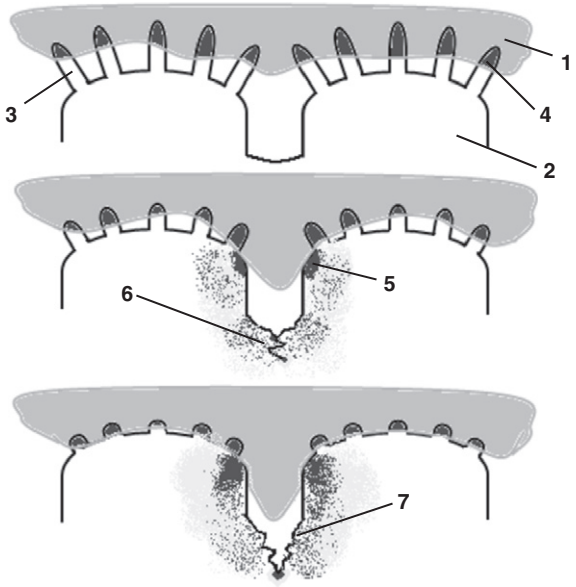

Fig. 5 – Mechanism for the superhydrophobic SiO_2 nanocomposite film surface morphological changes proceeding with the number of the icing/deicing experiments: (1) ice layer, (2) micrometer-scale feature, (3) nano-sized protrusion, (4) damaged part of nano-sized protrusion, (5) stress concentration (6) crack front formation and (7) further crack front propagation.

at high-humidity conditions. As a result, the adhesion force to ice grown from water vapor on such surfaces is expected to exceed the ice adhesion to smooth surfaces made of the same materials [25]. Additionally, superhydrophobic film/surface exposed to natural environment would quickly accumulate a thin layer of organic contaminants that would overcoat the original superhydrophobic surface altering its properties. However, with emerging new technologies in the area of surface modification, a very substantial part of ice adhesion and the corresponding van der Waals interactions can already be bypassed. For instance, in a recent study by P. Kim et al. it was shown that SLIPS-coated aluminum surfaces not only significantly reduce ice accumulation by allowing the condensed water droplets to slide off before they freeze but also enable the easy removal of the accumulated ice and melted water by gravity at low tilt angles [22].

4. Conclusions

Superhydrophobic SiO_2 nanocomposite films have been prepared on lithium aluminosilicate glass–ceramic substrates via modification with HMDS. Water droplet behavior on superhydrophobic films with water contact angle value of 162 ± 1° were examined during 30 surface icing/deicing cycles and changes in surface morphology and non-wetting characteristics were investigated. It has been demonstrated that the formation of the frozen water droplets with no further deformation and thawed water droplets with no further shape changes on superhydrophobic SiO_2 nanocomposite film is obtained faster as the number of icing/deicing cycles increases. After having been artificially iced and deiced 10 times, the superhydrophobic SiO_2 nanocomposite films demonstrated a water contact angle value of 146 ± 2° which effectively constitutes a non-superhydrophobic value. As the surface of superhydrophobic SiO_2 nanocomposite film is subjected to repetitive icing/deicing treatments, its surface skewness and kurtosis decrease indicating that nano-sized protrusions responsible for the non-wetting characteristics are damaged and spiky surface morphology is evolving into a bumpy one. The present work also suggests a mechanism for the superhydrophobic SiO_2 nanocomposite film surface morphological changes proceeding during the icing/deicing experiments.

Acknowledgments

The article was prepared under the support of the European Social Fund Agency implementing measure VP1-3.1-ŠMM-08-K of the Human Resources Development Operational Programme of Lithuania 2007–2013 3rd priority “Strengthening of capacities of researchers and scientists” (project No. VP1-3.1-ŠMM-08-K-01-013). A. Lazauskas gratefully acknowledges Support of the Research Council of Lithuania. Special thanks go to Dr. Rimantas Gudaitis from the Institute of Materials Science of Kaunas University of Technology.

REFERENCES

[1] Menini R, Farzaneh M. Advanced icephobic coatings. J Adhes Sci Technol 2011;25:971–92.
[2] Yan Y, Gao N, Barthlott W. Mimicking natural superhydrophobic surfaces and grasping the wetting process: a review on recent progress in preparing superhydrophobic surfaces. Adv Colloid Interface Sci 2011;169:80–105.
[3] Varanasi KK, Deng T, Smith JD, Hsu M, Bhate N. Frost formation and ice adhesion on superhydrophobic surfaces. Appl Phys Lett 2010;97:234102.
[4] Cao L, Jones AK, Sikka VK, Wu J, Gao D. Anti-icing superhydrophobic coatings. Langmuir 2009;25:12444–8.
[5] Sarkar D, Farzaneh M. Superhydrophobic coatings with reduced ice adhesion. J Adhes Sci Technol 2009;23:1215–37.
[6] Kulinich S, Farhadi S, Nose K, Du X. Superhydrophobic surfaces: are they really ice-repellent? Langmuir 2010;27:25–9.
[7] Nosonovsky M, Hejazi V. Why superhydrophobic surfaces are not always icephobic. ACS Nano 2012;6:8488–91.
[8] Wang J, Chen X, Kang Y, Yang G, Yu L, Zhang P. Preparation of superhydrophobic poly(methyl methacrylate)-silicon dioxide nanocomposite films. Appl Surf Sci 2010;257:1473–7.
[9] Manoudis PN, Karapanagiotis I, Tsakalof A, Zuburtikudis I, Panayiotou C. Superhydrophobic composite films produced on various substrates. Langmuir 2008;24:11225–32.
[10] Ogihara H, Katayama T, Saji T. One-step electrophoretic deposition for the preparation of superhydrophobic silica particle/trimethylsiloxysilicate composite coatings. J Colloid Interface Sci 2011;362:560–6.
[11] Xu GL, Deng C, Liang Y, Pi P, Hu J, Yang Z. Preparation of raspberry-like superhydrophobic SiO_2 particles by sol–gel method and its potential applications. Nanomater nanotechnol 2011;1:79–83.
[12] Stalder A, Kulik G, Sage D, Barbieri L, Hoffmann P. A snake-based approach to accurate determination of both contact points and contact angles. Colloids Surf A 2006;286:92–103.

[13] Tayebi N, Polycarpou A. Adhesion and contact modeling and experiments in microelectromechanical systems including roughness effects. Microsyst Technol 2006;12:854–69.
[14] Sedlaček M, Silva Vilhena LM, Podgornik B, Vižintin J. Surface topography modelling for reduced friction. Stroj Vestn-J Mech E 2011;57:674–80.
[15] Marmur A. Wetting on hydrophobic rough surfaces: to be heterogeneous or not to be? Langmuir 2003;19:8343–8.
[16] Bico J, Thiele U, Quéré D. Wetting of textured surfaces. Colloids Surf A 2002;206:41–6.
[17] Narhe R, González-Viñas W, Beysens D. Water condensation on zinc surfaces treated by chemical bath deposition. Appl Surf Sci 2010;256:4930–3.
[18] Wang J, Liu Z, Gou Y, Zhang X, Cheng S. Deformation of freezing water droplets on a cold copper surface. Sci China Ser E 2006;49:590–600.
[19] Liu Z, Gou Y, Wang J, Cheng S. Frost formation on a super-hydrophobic surface under natural convection conditions. Int J Heat Mass Transfer 2008;51:5975–82.
[20] Hashmi A, Strauss A, Xu J. Freezing of a liquid marble. Langmuir 2012;28:10324–8.
[21] Kulinich S, Farzaneh M. How wetting hysteresis influences ice adhesion strength on superhydrophobic surfaces. Langmuir 2009;25:8854–6.
[22] Kim P, Wong T-S, Alvarenga J, Kreder MJ, Adorno-Martinez WE, Aizenberg J. Liquid-infused nanostructured surfaces with extreme anti-ice and anti-frost performance. ACS Nano 2012;6:6569–77.
[23] Mishchenko L, Hatton B, Bahadur V, Taylor JA, Krupenkin T, Aizenberg J. Design of ice-free nanostructured surfaces based on repulsion of impacting water droplets. ACS Nano 2010;4:7699–707.
[24] Wier KA, McCarthy TJ. Condensation on ultrahydrophobic surfaces and its effect on droplet mobility: ultrahydrophobic surfaces are not always water repellant. Langmuir 2006;22:2433–6.
[25] Meuler AJ, McKinley GH, Cohen RE. Exploiting topographical texture to impart icephobicity. ACS Nano 2010;4:7048–52.